Article

Optimization of Dendritic Polypeptide Delivery System for Antisense Antibacterial Agents Targeting *ftsZ*

Yaoyao Li,[#] Yue Hu,[#] Zul Kamal, Yamiao Chen, Xiaoyan Xue, Shuting Yao, Hui Zhao, Min Jia, Yuan Li, Zheng Wang,* Mingkai Li,* and Zhou Chen*

Read Online

ACCESS | Metrics & More | Article Recommendations | SI Supporting Information

ABSTRACT: There is an urgent requirement for a novel treatment strategy for drug-resistant *Staphylococcus aureus* (*S. aureus*) infection. Antisense antimicrobials are promising antimicrobials, and efficient drug delivery systems are necessary for the further development of antisense antimicrobials. To develop new antisense drugs and further improve delivery efficiency and safety, we designed and screened new antisense sequences and optimized dendritic polypeptide nanoparticles (DP-AD) discovered in previous studies. The N/P ratio is optimized from 8:1 to 6:1, and the positive charge number of the optimized DP-AD is studied comprehensively. The results show that the N/P ratio and positive charge number have no significant effect on the particle size distribution and transport efficiency of DP-AD. Reducing the N/P ratio can significantly reduce the cytotoxicity of DP-AD, but it does not affect its delivery efficiency and antibacterial activity. However, in drug-resistant strains, the antibacterial activity of DP-AD7$_{6:1}$ with 10 positive charges is higher than that of DP-AD8$_{6:1}$ with 8 positive charges. Our research discovered a novel ASOs targeting *ftsZ* and concluded that DP-AD7$_{6:1}$ with 10 positive charges was the optimal choice at the current stage, which provided a promising strategy for the treatment of drug-resistant *S. aureus*.
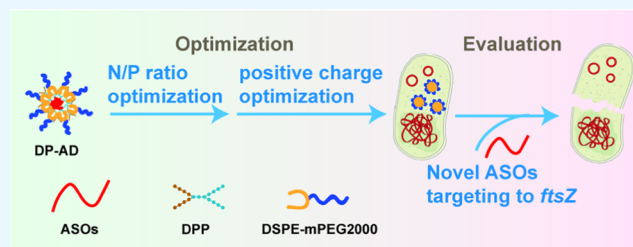
1. INTRODUCTION

In recent years, the rapid detection and reporting of drug-resistant bacteria caused by the abuse of antibiotics as well as the slow development of novel antibiotics have made it difficult for human beings to treat bacterial infections. *Staphylococcus aureus* (*S. aureus*), the leading cause of community-associated infections,[1] can lead to many lethal infectious diseases, such as endocarditis, pneumonia, and bacteremia.[2−4] What's worse, it has been reported that methicillin-resistant *S. aureus* (MRSA) accounts for about 25−50% of *S. aureus* infections in hospitals, leading to substantial morbidity and mortality and a huge economic burden.[5−7] To combat multidrug-resistant bacterial infections, many novel strategies have been developed, such as phage therapy, cationic antimicrobial peptides, and antibacterial polymers. However, these strategies face drawbacks such as effectiveness in complex infection, selectivity, toxicity, and stability.[8−12] Therefore, there is a pressing need to develop innovative antibacterial strategies for treating MRSA infections.

Antisense antimicrobials are macromolecular biologic drugs consisting of at least eight antisense oligonucleotides (ASOs) in length that bind to the target RNA and regulate RNA function through several different mechanisms.[13,14] ASOs exert antibacterial activity by interfering with the expression of targeted genes, such as the survival essential, virulence, or drug resistance-related genes, by the principle of complementary pairing of Watson−Crick nucleic acid bases.[15] Compared with

traditional antibiotic therapy, antisense antimicrobial agents have the advantages of a clear target, lower cytotoxicity, and a relatively fixed development model, which make a quick response to newly detected drug-resistant bacterial strains possible.[16−18] Antisense strategy has seen substantial progress in the treatment of mammalian disease, 10 antisense drugs have been approved by the FDA for the treatment of different types of diseases, for example, nusinersen for spinal muscular atrophy.[16,19] However, because of the high molecular weight and negative charges of the antisense cargos, the development of an antisense antibacterial strategy was relatively dropped behind and remained in laboratory research; a high-efficiency delivery system for ASOs in bacteria was the critical challenge that needed to be tackled.

The nanoparticle carriers are considered to be able to effectively improve the delivery efficiency of drugs in bacteria and enhance the antibacterial activity against drug-resistant strains.[20] Ye et al. found that combining antisense lncRNA of MDC1 and Oxaliplatin with cationic liposomes to form a

targeted co-delivery system could effectively improve the delivery efficacy of the cargos in cervical cancer,[21] but the low encapsulation rate and high cytotoxicity of liposomes made it difficult to further applied and studied in bacteria.[22−24] Tetrahedral DNA nanostructures were another novel antisense delivery system that had low cytotoxicity and immunogenicity. It has been reported that tetrahedral DNA could deliver ASOs into bacteria and inhibit bacterial gene expression in a concentration-dependent manner as a delivery system. However, the relatively low drug loading capacity, as well as the absence of the antisense effect *in vivo* and the safety study, limited the further study and application of this vehicle.[25−27] Cell-penetrating peptides attracted enormous interest as an ASOs delivery system as it could combine ASOs by both covalent and noncovalent methods. However, only neutral ASOs such as peptide nucleotide (PNA) could be delivered by the covalent method,[28] while the noncovalent method was limited by the poor stability and lower cellular uptake efficiency in bacteria.[29] In summary, the lack of a delivery system deeply hampered the further research and application of ASOs in bacteria.

Dendritic polypeptides (DPPs), as a dendritic hyper-branched structure, can be designed to be a more efficient drug transport vehicle by changing the functional group of the hydrophilic or hydrophobic region.[30] In our previous work, we designed a series of DPPs to form nanocomplexes with ASOs by noncovalent interaction, followed by stabilizing by DSPE-mPEG2000 to get the nanodelivery system (DP-AD). DP-AD7$_{8:1}$ and DP-AD8$_{8:1}$ were screened, which could effectively deliver ASOs into different bacterial strains and achieve effective antibacterial activity both *in vitro* and *in vivo*.[31] It has been reported that the number of positive charges and N/P ratio (the number of free amino groups in DPP to the number of nucleotides in ASOs) have a significant effect on the efficiency and cytotoxicity of the nanoparticle delivery system.[32−34] In order to explore new antisense targets, further improve the delivery efficiency, and decrease the toxicity of DP-AD, a novel ASOs targeting filamentous temperature-sensitive mutant Z (*ftsZ*), a survival essential gene encoding a filamentous GTP enzyme in bacteria,[35,36] was designed and screened against *S. aureus* (ATCC29213) and MRSA (USA300 LAC). Furthermore, we optimized the N/P ratio of DP-AD from 8:1 to 6:1 and comprehensively studied the influence of positive charge numbers on the properties of the nanoparticles. In summary, our research discovered a new antisense sequence, and the optimized DP-AD7$_{6:1}$ showed lower cytotoxicity and similar antibacterial activity, which shed light on the further optimization of DPP.

2. MATERIALS AND METHODS

2.1. Materials and Reagents.
Dendritic polypeptides 7 (DPP7) and DPP8 (Table S1) were synthesized by China Peptides Co., Ltd. (Suzhou, China). Phosphorothioate-modified ASOs, 5′-fluorescein amidites (FAM)-labeled ASOs, and primers were synthesized by Sangon Biotech (Shanghai, China). 1,2-Distearoyl-*sn*-glycero-3-phosphoethanol-amine-*N*-methoxy (poly(ethylene glycol))-2000 (DSPE-mPEG2000) was purchased from Xi'an ruixi Biological Technology Co., Ltd. Lipofectamine 2000 was obtained from Life Technologies (Invitrogen, CA). Bacterial strains *Staphylococcus aureus* (*S. aureus* ATCC29213) and methicillin-resistant *S. aureus* (MRSA) (USA300 LAC), mouse brain capillary endothelial cell line (Bend.3) and human nonsmall cell lung cancer cell

line (A549) were stored in our laboratory. FM4−64 was purchased from Life Technologies (Invitrogen, CA).

2.2. Design and Screening of ASOs Sequences Targeting to *ftsZ*.
The sequences of *ftsZ* of *S. aureus* (ATCC29213) and MRSA (USA300 LAC) were searched in GENBANK. After BLAST alignment, RNA structure 6.4 was used to predict the secondary structure of *ftsZ* mRNA, and a series of possible ASOs were designed and synthesized. Then, the optimal ASOs sequence was obtained according to the bacterial growth curve experiment (Section 2.7).

2.3. Preparation of the NPs.
One micromolar DP-AD7$_{6:1}$ and DP-AD8$_{6:1}$ were prepared according to the previous work.[31] Briefly, 2.25 μL of DPP and 15 μL of ASOs (20 μM) were mixed by vertexing for 1 min at 2600 rpm and incubating for 30 min at 37 °C to get the DPP/ASOs nanocomplex. Then, DSPE-mPEG2000 was added to the solution, followed by vortexing and incubation, similar to the previous step. DP-AD with different N/P ratios and concentrations were prepared by adjusting the molar amount of DPP. LF2000-NPs were prepared strictly in accordance with the protocol described in our previous study.[31]

2.4. Characterization of the NPs.
The preparation of 1 mL of DP-AD with a concentration of 1 μM required 7.5 μL of DPPs with 50 μL (20 μM) of ASOs and 25 μL of DSPE-mPEG2000, and then the particle size, zeta potential, and polydispersity index (PDI) were measured by a dynamic light scattering meter (DLS, Marlvern Panalytical, U.K.).

Transmission electron microscopy (TEM) was adapted to observe the morphology and solid size of DP-AD. Twenty micromolar DP-AD with an N/P ratio of 8:1 and 6:1 were prepared as mentioned above and dropped to the copper mesh after by depositing for 5 min and evaporating for 2 min at room temperature. Then, the NPs were observed by magnifying $10^5\times$ at 80 kV voltage.

Fluorescence spectrophotometry was used to measure the encapsulation efficiency. First, the FAM-labeled ASOs solution was scanned by a fluorescence spectrophotometer to determine the maximum excitation and emission wavelength, and then the fluorescence intensity of the FAM-labeled ASOs solution with a concentration ranging from 0.03 to 1 μM was measured to establish a standard curve. Second, 1 μM DPP/ASOs was prepared and centrifuged at 14,000g for 30 min, the fluorescence intensity of the supernatant was measured, and then the encapsulation efficiency of ASOs could be calculated.

2.5. Cytotoxicity Assessment *In Vitro*.
One hundred microliters of aliquot of Bend.3 and A549 cells in high-glucose DMEM with 10% fetal bovine serum and 1% penicillin/streptomycin were inoculated in a 96-well culture plate with 1 × 10^5/mL and cultured at 37 °C and 5% CO_2 for 24 h to ensure cell adhesion. Then, the medium was replaced with fresh culture medium, followed by adding DP-AD into the culture medium to achieve a final concentration of 1 and 4 μM, respectively. After incubating for 24 h, the original culture medium was removed, CCK-8 solution was added to each well, and incubated in a 5% CO_2 incubator for 1 h. The absorbance of each well was measured by enzyme-linked immunosorbent assay (Bio Rad) at 450 nm, and the cell survival rate was calculated. The cell without any treatment was used as a control.

2.6. Delivery Efficiency of the DP-AD Delivery System.
FAM-labeled ASOs were used to prepare DP-AD solutions with different N/P ratios. Three hundred microliters of DP-AD was mixed with the same volume of *S. aureus*

(ATCC29213) and MRSA (USA300 LAC) solution (10^6 CFU/mL), respectively. Then, the mixtures were incubated at 37 °C for 1 h and centrifuged at 2500g for 5 min. Then, the supernatant was discarded and the mixture was washed with 500 μL of PBS twice and resuspended with 100 μL of PBS. BL 1 channel (green) of flow cytometry (Bioscience) was adapted to detect the positive ratio of bacteria (that is, bacterial FAM positive). The experimental results were analyzed using Flow Jo 10.6.2. LF2000-NPs were used as a positive control and free FAM-labeled ASOs were used as the negative control.

Three hundred microliters of FAM-labeled DP-ADs (0.5 μM) were mixed with 100 μL of 10^8 CFU/mL S. aureus (ATCC29213) and MRSA (USA300 LAC) solution, respectively, and incubated for 0.5 h at 37 °C in the absence of light. The mixture was then centrifuged at 5000g for 5 min, washed, and resuspended twice with 500 μL of PBS, followed by a final resuspension in 100 μL PBS. Five microliters of FM4−64 (200 μg/mL) was incubated with the bacterial solutions for 1 min on ice for staining. After centrifuging and washing twice with 500 μL PBS, the bacteria were resuspended in 50 μL of PBS. Then, 10 μL of the bacterial solution was applied onto a slide, air-dried, and sealed with 5 μL of a tablet sealant and then observed by using lattice-structured illumination microscopy (SIM, Elyra 7).

2.7. Bacterial Growth Curve Experiment. Three hundred μmicroliters of aliquot of DP-AD solutions with concentrations ranging from 0.5 to 4 μM were mixed with 3 × 10^6 CFU bacteria in 300 μL of TSB broth. Then, the mixture was added to three wells averagely to the 100-well culture plate specially used for the growth curve instrument (Bio screen C Company, U.K.) and cultured at 37 °C for 18−20 h. The absorbance of $OD_{600\ nm}$ was measured per hour to get the growth curve. A 0.5 μg/mL oxacillin[37] was used as a positive control against S. aureus (ATCC29213) and MRSA (USA300 LAC), respectively. Free ASOs were used as a negative control. The normal bacterial growth group was used as a control.

2.8. RT-PCR. According to the gene sequence of ftsZ and 16 s rRNA of S. aureus reported in the Genebank, the primers were designed and synthesized by Sangon Biotech Co., Ltd. The primers used were as follows: S. aureus 16 s rRNA forward 5′-GCTGCCCTTTGTATTGTC-3′ and reverse 5′-AGATGTTGGGGTTAAGTCCC-3′, ftsZ forward 5′-ATCGC-TATCAACACAGACGGTCAAG-3′ and reverse 5′-TAC-CAGTTCCGCCACCCATACC-3′. The bacterial solution (about 3 × 10^6 CFU) was incubated with 1 μM DP-AD at 37 °C for 4 h. Total bacterial RNA was extracted by Trizol (Invitrogen Company, California). RNA was reverse transcribed using a reverse transcription kit and quantitative kit (Mei5 Biotechnology Co., Ltd.), and then the cDNA was quantified by a real-time Q-PCR system (Mx3005P, Agilent Stratagene, La Jolla, CA). All of the operations were carried out strictly according to the operation protocol. The normal bacterial growth group was used as a control.

2.9. Statistical Analysis. Results were expressed as mean ± SD. Statistical significance was performed with GraphPad Prism 8.3.0. Differences between the two groups were compared using t tests.

3. RESULTS

3.1. Design and Screening of ASOs Sequences Targeting to ftsZ. BLAST alignment results showed that the homology in different S. aureus strains of ftsZ, an essential gene for the growth of bacteria, was up to 99% (Table S2 and Figure S1), indicating that ftsZ was an appropriate target gene. RNA structure 6.4 was used to predict the secondary structure of ftsZ (Figure 1A), 7 antisense sequences were designed based
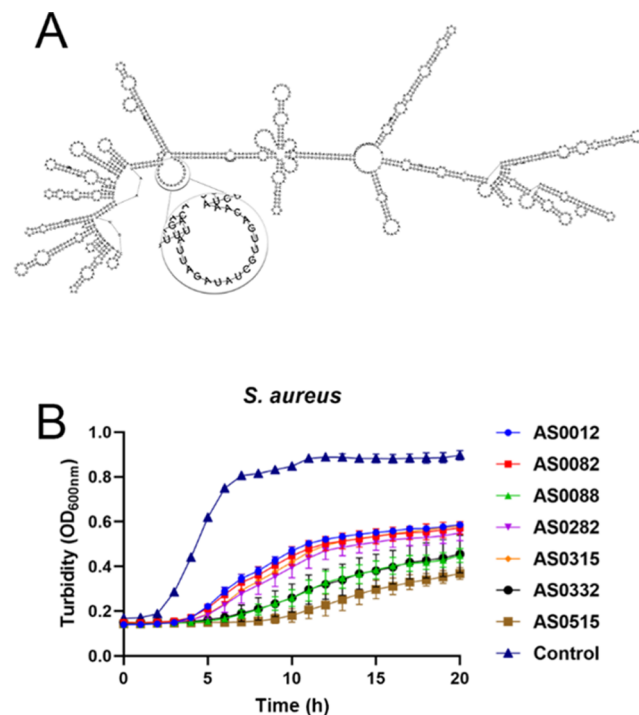
Figure 1. Design and screening of antisense oligodeoxynucleotides sequences. (A) Secondary structure of ftsZ of S. aureus and gene fragment to which antisense sequence AS0515 complementary. (B) The growth curve of S. aureus treated with 1 μM DP-AD was prepared by the designed ASOs sequences. The optimal antisense sequence was AS0515. The bacterial growth group without any treatment was used as a control.

on the principle of minimum free energy (Table S3), and the growth curve experiment was adopted to screen the antisense sequence with the best inhibitory effect. Finally, AS0515, targeting the free region in the secondary structure of ftsZ (Figure 1A), showed the highest antisense antibacterial activity, which was used in the follow-up experiment (Figure 1B).

3.2. Optimization of DP-AD. Our group previously designed a series of dendritic polypeptides (DPPs) as carriers to deliver ASOs into bacteria. DPP formed spherical DPP/ASOs nanoparticles with 10-nucleotide ASOs by electrostatic and hydrophobic interactions, followed by decoration by DSPE-mPEG2000 to form a DP-AD delivery system. As a result, the amphipathic DPP7 and DPP8 containing 8−10 positive charges and 2 histidine residues showed high delivery efficiency and antisense antibacterial activity both in vitro and in vivo.[26,31] It has been reported that the N/P ratio significantly influences the delivery efficiency and cytotoxicity of nanoparticles.[33,34] Meanwhile, the number of positive charges on the surface of nanoparticles would influence the interactions of nanoparticles with the negative charges on the bacterial cell membrane, which further influenced the delivery efficiency and cytotoxicity.[32,38,39] To optimize the DP-AD delivery system, we decreased the N/P ratio from 8:1 to 6:1 and comprehensively compared DP-AD7$_{6:1}$ and DP-AD8$_{6:1}$, which contained 10 and 8 positive amine acid residues, to
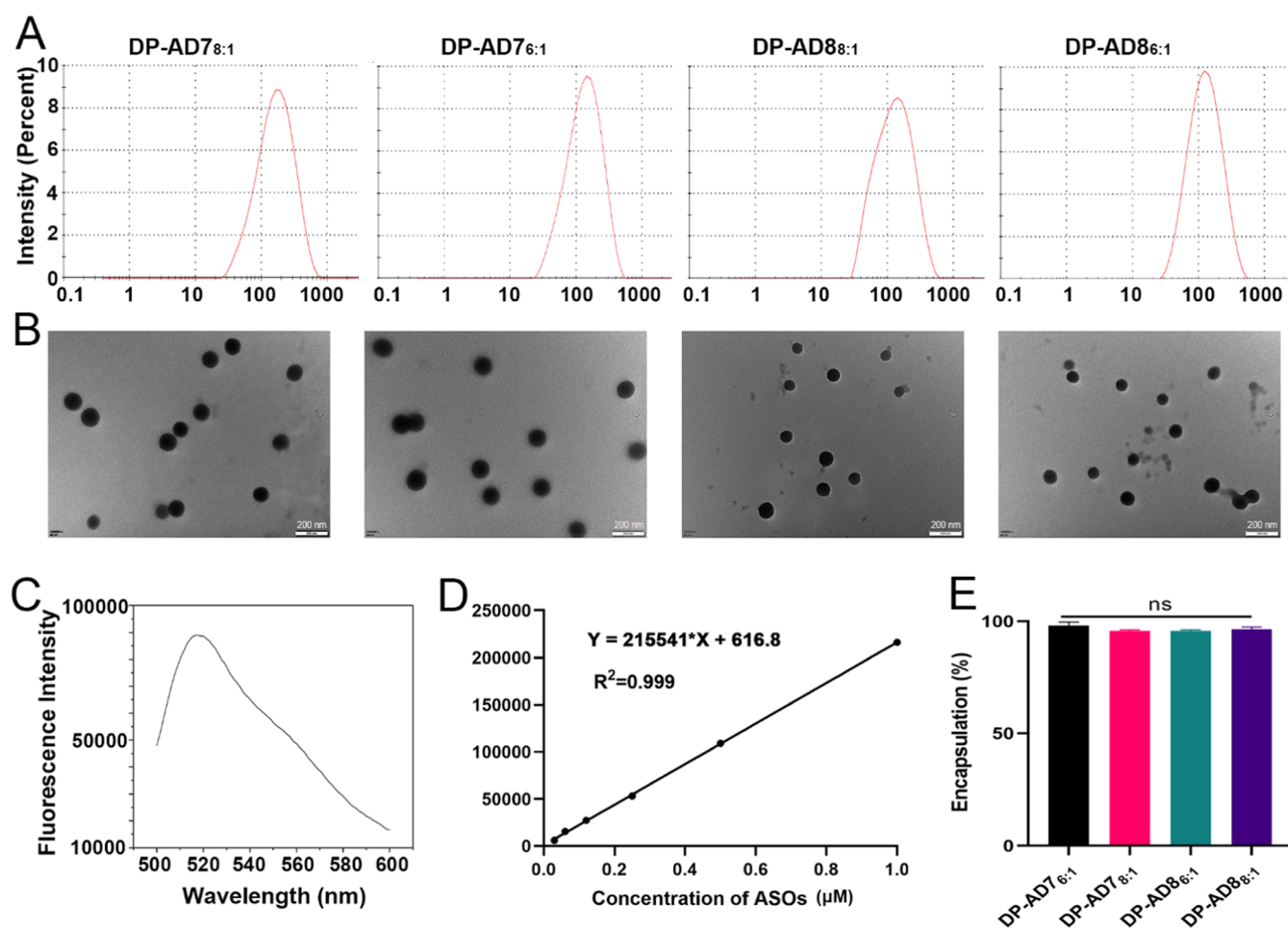
Figure 2. Characterization of DP-AD. (A) Particle size of DP-AD with different N/P ratios were determined by DLS. (B) Morphology and solid size of DP-AD detected by TEM. Scale bars: 200 nm. (C) Fluorescence spectra of 0.5 μM free ASOs. (D) Standard curves of ASOs measured by fluorescence spectrophotometer. (E) Encapsulation efficiency of ASOs by DPP with different of N/P ratios as well as different positive charges measured by fluorescence spectrophotometry.

further study the influence of N/P and positive charge number on the delivery efficiency and safety of DP-AD.

3.3. Characterization of DP-AD. DP-ADs with different N/P ratios were prepared by two-step protocols as described above. The DLS results showed that the size of DP-AD7$_{6:1}$ and DP-AD8$_{6:1}$ were both less than 150 nm, PDI (polydispersion index) was less than 0.4, the ζ potentials were between 14.5 and 17.3 mV (Figure 2A and Table S4). TEM further showed that the nanoparticles with different N/P ratios were spherical, with diameters smaller than 100 nm (Figure 2B and Table S4). Further, both the results showed that the size of DP-AD8$_{6:1}$ was slightly smaller than that of DP-AD7$_{6:1}$, while the change of the N/P ratio had little effect on the particle size and morphology in the nanoparticles (Figure S1). The fluorescence spectra of 0.5 μM free ASOs showed that the maximum excitation wavelength and maximum emission wavelength were approximately 488 and 517 nm, respectively (Figure 2C). Fluorescent spectrophotometry was adapted to measure the encapsulation of ASOs, and the results indicated that the encapsulation efficiency was all above 90% (Figure 2D,E), showing no significant difference between different DP-AD with different N/P ratios.

3.4. Cytotoxicity of DP-AD. CCK-8 assay was adapted to detect the cytotoxicity of DP-AD in Bend.3 and A549 cells. After treatment with DP-AD7$_{6:1}$ or DP-AD8$_{6:1}$, the viability of these cells was significantly increased compared with DP-AD7$_{8:1}$ and DP-AD8$_{8:1}$. Also, at its concentration of 1 μM, there was no significant difference from the control. However, cell viability decreased significantly with the concentration of nanoparticles increasing from 1 to 4 μM but remained above 70% (Figure 3). These results showed that reducing the ratio of N/P is beneficial to cell viability, and there is no significant difference in the cytotoxicities of DP-AD7$_{6:1}$ and DP-AD8$_{6:1}$, which initially improves the safety of antisense antimicrobial agents.

3.5. Delivery Efficiency of ASOs by DP-AD. As reported, the N/P ratios would impair the delivery efficacy of polypeptide delivery system.[34] We investigated whether reduced N/P in the DP-AD affected the delivery efficiency of ASOs in bacteria. Flow cytometry results showed that the positive rates of both *S. aureus* (ATCC29213) and USA300 LAC treated with DP-AD with different N/P ratios were greater than 90%. As a positive control, LF2000-NPs have roughly the same delivery efficiency as DP-AD (Figure 4). To further confirm the potential of DP-AD to carry ASOs into bacteria, live imaging was conducted using an Elyra 7 microscope with a 63×/1.46 oil immersion objective. The captured images were processed using SIM by Zeiss Zen Black software. After incubation with FAM-labeled DP-AD in the dark for 0.5 h, strong green fluorescence was observed in the
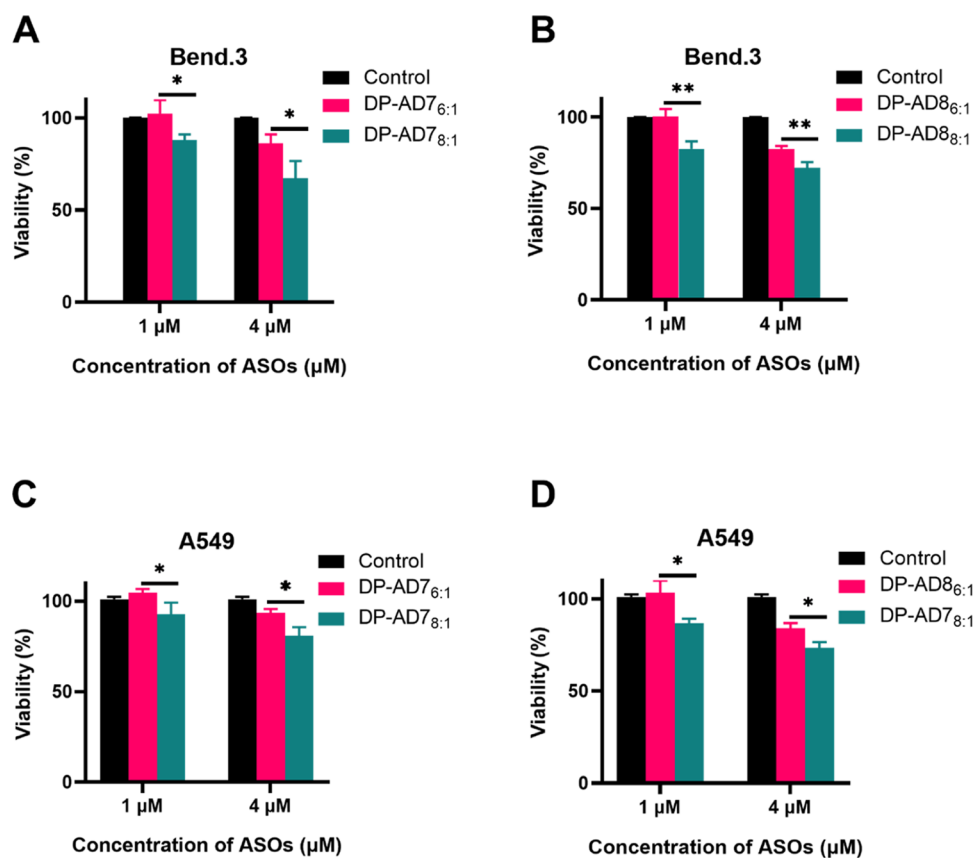
Figure 3. Cytotoxicity of DP-AD. (A, B) Viability of Bend.3 cells treated with different concentrations of DP-AD. (C, D) Viability of A549 cells treated with different concentrations of DP-AD. *$P < 0.05$, **$P < 0.01$.

cytoplasm of both bacteria (Figure 5). Collectively, reducing the N/P from 8:1 to 6:1 does not affect the delivery of DP-AD.

3.6. Antibacterial Efficacy of DP-AD In Vitro. In order to verify the antibacterial efficacy of the nanoparticles, DP-AD7$_{6:1}$ and DP-AD8$_{6:1}$ targeting $ftsZ$ were prepared to measure the growth curve of S. aureus (ATCC29213) and MRSA (USA300 LAC). The results showed that DP-AD7$_{6:1}$ and DP-AD8$_{6:1}$ could effectively inhibit the growth of S. aureus (ATCC29213) in a concentration-dependent manner (Figure 6A,B). DP-AD7$_{6:1}$ and DP-AD8$_{6:1}$ showed a lower antibacterial activity in USA300 LAC, in which DP-AD7$_{6:1}$ needed a higher concentration, up to 4 μM, to entirely inhibit the bacterial growth, while DP-AD8$_{6:1}$ did not show significant antibacterial activity with the same concentration (Figure 6C,D). Thus, the antibacterial activity of DP-AD7$_{6:1}$ was better than that of DP-AD8$_{6:1}$, although the antibacterial activity of DP-AD7$_{6:1}$ was similar to that of DP-AD8$_{6:1}$ in sensitive strains.

To further confirm the antibacterial activity of DP-AD, RT-PCR was adapted to detect the $ftsZ$ expression of S. aureus (ATCC29213) and USA300 LAC treated by DP-AD targeting $ftsZ$. The results showed that DP-AD7$_{6:1}$ could significantly inhibit the expression of targeted genes in S. aureus (ATCC29213) in a concentration-dependent manner compared to the mismatch group, which was basically consistent with the growth curve results. DP-AD8$_{6:1}$ also showed similar results to growth curve results, namely, significant inhibition of the $ftsZ$ gene expression was observed in S. aureus (ATCC29213) but not in the USA300 LAC (Figure 7). Collectively, DP-AD7$_{6:1}$ with 10 positive charges showed significant antibacterial activity in both S. aureus

(ATCC29213) and USA300 LAC, while DP-AD8$_{6:1}$ with 8 positive charges could only inhibit the growth and gene expression of S. aureus (ATCC29213) but showed no significant activity in the drug-resistant USA300 LAC.

4. DISCUSSION

As the increasing detection rate of multidrug-resistant S. aureus, the need for developing a novel antimicrobial strategy is urgent. Antisense antibacterial agent was a promising strategy for drug-resistant bacterial infection because of advantages such as high specificity and quick response for new drug-resistant bacterial strains. The significant progress in mammalian cells has revitalized the antisense antibacterial strategy.[40] However, the further development and application of the antisense antibacterial strategy was limited by the delivery system. We showed that the amphipathic DPP7 and DPP8 with 8−10 positive charges and 2 histidine residues could effectively encapsulate and deliver ASOs into different bacteria and further exhibited antisense antibacterial activity in our previous study.[31]

The ideal target gene of ASOs should be the key gene for bacterial survival or the drug-resistant related gene as well as have high homology. Several novel antisense antibacterial agents, such as PPNA06 and PS-ODN04, could inhibit bacterial growth or restore the sensitivity to antibiotics by targeting survival essential gene $rpoD$ or the drug-resistant gene $mecA$, respectively.[41,42] $ftsZ$ codes the filamentous GTP enzyme, a survival essential protein in S. aureus, and had homology up to 99% in different S. aureus strains, indicating that this gene was an appropriate target of ASOs. AS0515,
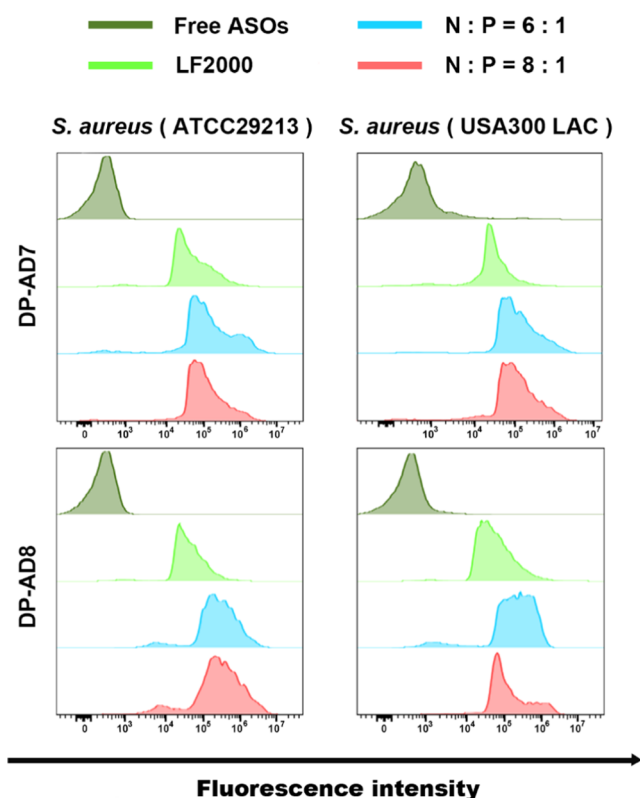
Figure 4. Positive rates of bacteria treated with DP-AD with different N/P ratios measured by flow cytometry, with free ASOs and LF2000-NPs used as negative and positive controls, respectively.

which is complementary to the free region in the RNA secondary structure of *ftsZ*, showed satisfactory antibacterial activity and was a promising antisense antibacterial agent against drug-resistant *S. aureus*.

It has been reported that the number of positive charges in peptides and the N/P ratio were the two key factors for the delivery efficiency and safety of a nanoparticle delivery system.[34,39] The higher N/P ratio and more positive charges in CPP were beneficial for the encapsulation and transfection

efficiency, while the decrease of positive charges in CPP or N/P ratio could decrease the cytotoxicity.[33,43] To further improve the delivery efficiency and safety performance, the N/P ratio of DP-AD was optimized, and the influence of the number of positive charge amino acid residues was comprehensively studied. When the N/P ratio was optimized from 8:1 to 6:1, the cytotoxicity of DP-AD decreased significantly. We also tried to decrease the N/P ratio to 4 or less, but the ASOs could not effectively encapsulate DPP to form stable nanoparticles.[31] Although DP-AD7$_{6:1}$ and DP-AD8$_{6:1}$, which showed similar safety profiles with both N/P ratios, showed similar delivery capabilities, DP-AD7 with 10 positive charge numbers showed higher antibacterial activity than DP-AD8 with 8 positive charges, which was consistent with the previous reports.[38] These results provided a direction for the design of DPP.

TEM and DLS measured the different diameters of nanoparticles. When measured by TEM, the nanoparticles were dried, and we observed the solid state of the particles. However, the diameter measured by DLS was the hydrodynamic diameter. Generally, the solid diameter of organic nanoparticles, such as the cell-penetrating peptides and liposomes, was smaller than the hydrodynamic diameters because of the dehydration process involved in the preparation process.[44] We also found that the particle size and morphology of DP-AD8$_{6:1}$ are slightly smaller than that of DP-AD7$_{6:1}$, which might be due to the influence of the positive charge number. The PDI, the parameter to evaluate the size distribution of nanoparticles, was less than 0.4, indicating that the dispersion of nanoparticles was relatively uniform.[24,45] After reducing the N/P ratio, the particle size, morphology of DP-AD, and the encapsulation rate of ASOs had no significant influence; flow cytometry also showed no significant difference between the nanoparticles with the N/P ratios of 6:1 and 8:1. These results indicated that decreasing the N/P ratio from 8:1 to 6:1 did not influence the formation and delivery capacity of DP-AD.

The growth curve and RT-PCR results showed that DP-AD7$_{6:1}$ had higher antibacterial activity than DP-AD8$_{6:1}$ in the drug-resistant USA300 LAC, which had a complex drug-resistant mechanism, although these two nanoparticles had
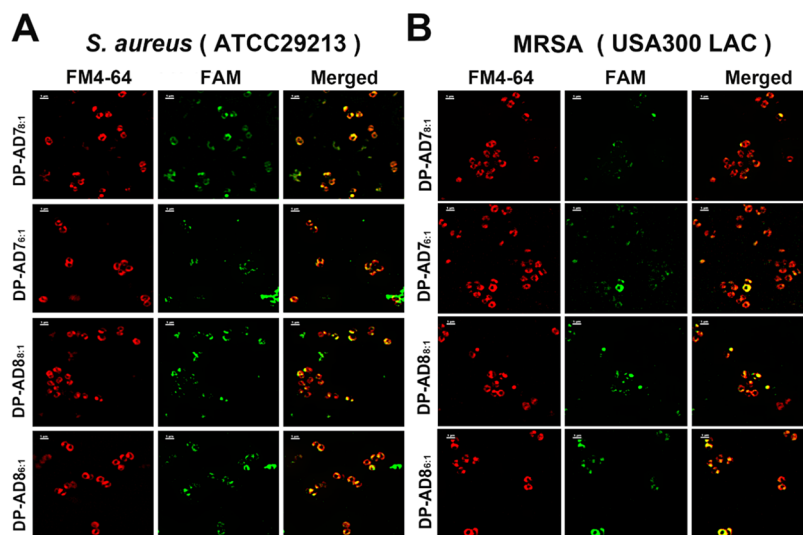
Figure 5. Elyra 7 with Lattice SIM was used to observe the uptake of DP-AD by different bacteria. (A) Uptake of DP-AD by *S. aureus* (ATCC29213). (B) Uptake of DP-AD by MRSA (USA300, LAC). Scale bars: 1 μm.
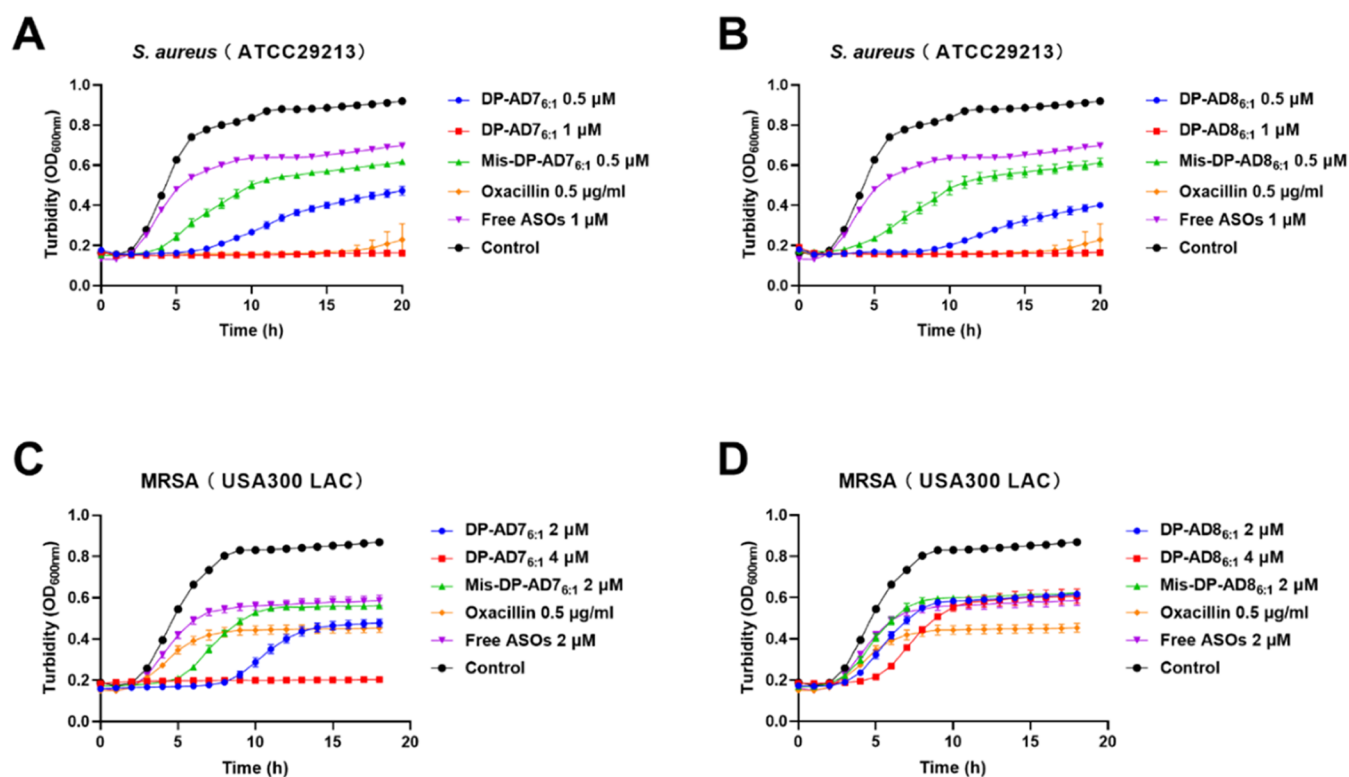
Figure 6. Growth of bacteria treated with DP-AD. (A, B) Growth inhibition of *S. aureus* (ATCC29213) by DP-AD7$_{6:1}$ (A) and DP-AD8$_{6:1}$ (B) at different concentrations. (C, D) Growth inhibition of DP-AD7$_{6:1}$ (C) and DP-AD8$_{6:1}$ (D) on drug-resistant bacteria MRSA (USA300 LAC). Free ASOs and oxacillin were used as negative and positive controls, respectively. The bacterial growth group without any treatment was used as a control.
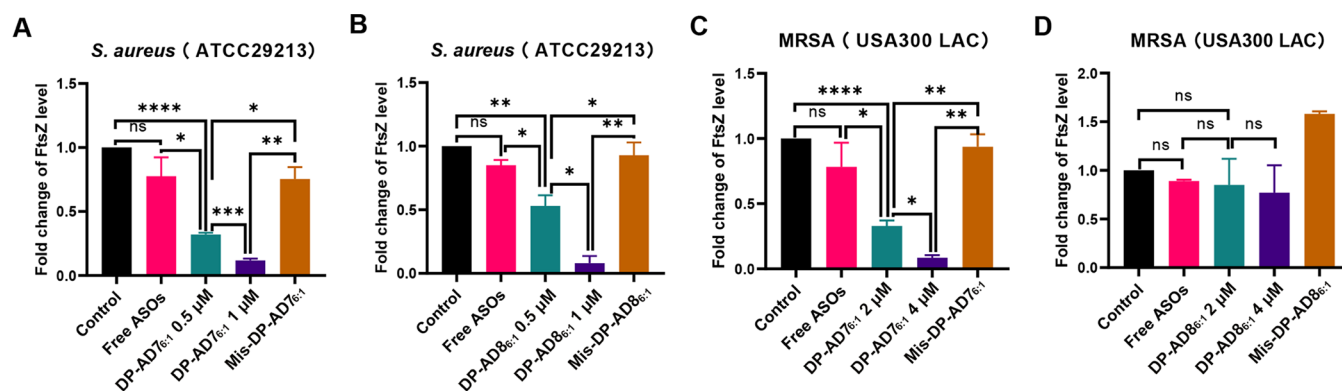
Figure 7. Gene expression of *ftsZ* treated with DP-AD. The inhibition of *ftsZ* expression of *S. aureus* (A, B) and MRSA (USA300 LAC) (C, D) treated with different concentrations of different DP-AD. Free ASOs wrere used as a negative control. The normal bacterial growth group was used as a control. *$P < 0.05$, **$P < 0.01$, ***$P < 0.001$, ****$P < 0.0001$.

similar antisense antibacterial activities in *S. aureus*. There are two possibilities to explain these results. First, the number of positive charge amino acid residues plays a decisive role in the antibacterial activity of the nanoparticles. Then, USA300 LAC has a complex drug-resistant mechanism, which may increase the excretion or degradation of DP-AD or ASOs.[10] However, the concrete mechanism remains to be further studied.

In summary, we designed and screened novel ASOs targeting *ftsZ*, which showed satisfactory antisense antibacterial activity. Then, we optimized the DP-AD delivery system to improve its delivery efficiency and safety. The influence of the N/P ratio and the number of positive charges on delivery efficiency and safety have been studied deeply. The N/P ratio had no obvious influence on the formation of DP-AD, as well

as the delivery efficiency in the tested bacterial strains; however, the decrease in the N/P ratio could significantly improve the safety of the nanoparticles to mammalian cells. DPP with 8 or 10 positive charges had similar nanoparticle profiles of size, ζ potential, delivery efficiency, and safety. However, DP-AD7$_{6:1}$ with 10 positive charges had a higher antibacterial activity than that of DP-AD8$_{6:1}$ with 8 positive charges in the drug-resistant strain. Collectively, we screened a new ASOs targeting *ftsZ*, and DP-AD7$_{6:1}$ was the optimal choice at this stage, which may provide a new idea for the treatment of drug-resistant strains. In the future, we will optimize the structure and sequence of DPP7 to further improve its delivery efficiency and safety. In addition, the mechanism of the influence of the positive charges of DP-AD

on the antibacterial activity in drug-resistant bacteria was another essential issue to be studied with the aim to provide a turnkey platform for the treatment of drug-resistant bacteria.

◼ ASSOCIATED CONTENT

ⓢ Supporting Information

The Supporting Information has been uploaded separately in the submission system. The Supporting Information is available free of charge at https://pubs.acs.org/doi/10.1021/acsomega.4c00114.

Basic information on DPP7 and DPP8 (Table S1); list of *ftsZ* homologues in other *Staphylococcus aureus* compared to ATCC29213 (Table S2); the antisense regions of *ftsZ* of *S. aureus* (ATCC29213 and USA300 LAC) were compared by BLAST (Figure S1); ASOs sequences (Table S3); size and potential of DP-AD nanoparticles (Table S4); and particle size of DP-AD with different N/P ratios measured by DLS and TEM (Figure S2) (PDF)

◼ AUTHOR INFORMATION

Corresponding Authors

Zheng Wang − *College of Pharmacy, Shaanxi University of Chinese Medicine, Xi'an 712046, China;*
Email: wazh0405@126.com

Mingkai Li − *College of Pharmacy, Shaanxi University of Chinese Medicine, Xi'an 712046, China; Department of Pharmacology, School of Pharmacy, The Fourth Military Medical University, Xi'an 710032, China;* Email: mingkai@fmmu.edu.cn

Zhou Chen − *Department of Pharmacology, School of Pharmacy, The Fourth Military Medical University, Xi'an 710032, China;* ⓘ orcid.org/0000-0002-9500-0884; Phone: +86 29 8477 4555; Email: chenzhou_cky@163.com

Authors

Yaoyao Li − *College of Pharmacy, Shaanxi University of Chinese Medicine, Xi'an 712046, China; Department of Pharmacology, School of Pharmacy, The Fourth Military Medical University, Xi'an 710032, China*

Yue Hu − *Department of Pharmacology, School of Pharmacy, The Fourth Military Medical University, Xi'an 710032, China*

Zul Kamal − *Department of Pharmacy, Shaheed Benazir Bhutto University, Sheringal 18000 Khyber Pakhtunkhwa, Paksitan; School of Pharmacy, Shanghai Jiao Tong University, Shanghai 200240, China*

Yamiao Chen − *Department of Pharmacology, School of Pharmacy, The Fourth Military Medical University, Xi'an 710032, China*

Xiaoyan Xue − *Department of Pharmacology, School of Pharmacy, The Fourth Military Medical University, Xi'an 710032, China;* ⓘ orcid.org/0000-0001-6646-8253

Shuting Yao − *College of Pharmacy, Shaanxi University of Chinese Medicine, Xi'an 712046, China; Department of Pharmacology, School of Pharmacy, The Fourth Military Medical University, Xi'an 710032, China*

Hui Zhao − *Department of Pharmacology, School of Pharmacy, The Fourth Military Medical University, Xi'an 710032, China*

Min Jia − *Department of Pharmacology, School of Pharmacy, The Fourth Military Medical University, Xi'an 710032, China*

Yuan Li − *Medical College, Xi'an Peihua University, Xi'an 710061, China*

Complete contact information is available at:
https://pubs.acs.org/10.1021/acsomega.4c00114

Author Contributions

[#]Y.L. and Y.H. contributed equally to this work and share the first authorship. Y.L., Y.C., H.Z., and Y.L. completed these experiments together. Y.H., X.X., and Z.K. processed the experimental data. S.Y. participated in the cell and bacterial culture experiments. M.J. provided the experimental support. Z.C. revised the manuscript. M.L. and Z.W. were responsible for project management and summary. All authors contributed to this article and approved the submissions.

Notes

The authors declare no competing financial interest.

◼ ACKNOWLEDGMENTS

◼ REFERENCES

(1) Lee, A. S.; de Lencastre, H.; Garau, J.; Kluytmans, J.; Malhotra-Kumar, S.; Peschel, A.; Harbarth, S. Methicillin-resistant *Staphylococcus aureus*. *Nat. Rev. Dis. Primers* **2018**, *4*, No. 18033, DOI: 10.1038/nrdp.2018.33. Published Online: May. 31, 2018

(2) Guo, Y.; Song, G.; Sun, M.; Wang, J.; Wang, Y. Prevalence and Therapies of Antibiotic-Resistance in *Staphylococcus aureus*. *Front. Cell. Infect. Microbiol.* **2020**, *10*, No. 107, DOI: 10.3389/fcimb.2020.00107. Published Online: Mar. 17, 2020

(3) Kawada-Matsuo, M.; Le, M. N.-T.; Komatsuzawa, H. Antibacterial Peptides Resistance in *Staphylococcus aureus*: Various Mechanisms and the Association with Pathogenicity. *Genes* **2021**, *12* (10), No. 1527, DOI: 10.3390/genes12101527.

(4) Kwiecinski, J. M.; Horswill, A. R. *Staphylococcus aureus* bloodstream infections: pathogenesis and regulatory mechanisms. *Curr. Opin. Microbiol.* **2020**, *53*, 51−60. Published Online: Mar. 12, 2020

(5) Lakhundi, S.; Zhang, K. Methicillin-Resistant *Staphylococcus aureus*: Molecular Characterization, Evolution, and Epidemiology. *Clin. Microbiol. Rev.* **2018**, *31* (4), No. e00020-18, DOI: 10.1128/CMR.00020-18.

(6) Rungelrath, V.; DeLeo, F. R. *Staphylococcus aureus*, Antibiotic Resistance, and the Interaction with Human Neutrophils. *Antioxid. Redox Signaling* **2021**, *34* (6), 452−470. Published Online: Jun. 23, 2020

(7) Hassoun, A.; Linden, P. K.; Friedman, B. Incidence, prevalence, and management of MRSA bacteremia across patient populations-a review of recent developments in MRSA management and treatment. *Crit. Care* **2017**, *21* (1), No. 211, DOI: 10.1186/s13054-017-1801-3. Published Online: Aug. 14, 2017

(8) Lin, D. M.; Koskella, B.; Lin, H. C. Phage therapy: An alternative to antibiotics in the age of multi-drug resistance. *WJGPT* **2017**, *8* (3), 162.

(9) Lin, B.; Li, R.; Handley, T. N.; Wade, J. D.; Li, W.; O'Brien-Simpson, N. M. Cationic Antimicrobial Peptides Are Leading the Way to Combat Oropathogenic Infections. *ACS Infect. Dis.* **2021**, *7* (11), 2959−2970.

(10) Li, W.; Separovic, F.; O'Brien-Simpson, N. M.; Wade, J. D. Chemically modified and conjugated antimicrobial peptides against superbugs. *Chem. Soc. Rev.* **2021**, *50* (8), 4932−4973.

(11) Kenawy, E.-R.; Worley, S. D.; Broughton, R. The Chemistry and Applications of Antimicrobial Polymers: A State-of-the-Art Review. *Biomacromolecules* **2007**, *8* (5), 1359−1384.

(12) Ma, B.; Fang, C.; Lu, L.; Wang, M.; Xue, X.; Zhou, Y.; Li, M.; Hu, Y.; Luo, X.; Hou, Z. The antimicrobial peptide thanatin disrupts the bacterial outer membrane and inactivates the NDM-1 metallo-β-lactamase. *Nat. Commun.* **2019**, *10* (1), No. 3517, DOI: 10.1038/s41467-019-11503-3.

(13) Bennett, C. F. Therapeutic Antisense Oligonucleotides Are Coming of Age. *Annu. Rev. Med.* **2019**, *70*, 307−321.

(14) Bennett, C. F.; Swayze, E. E. RNA targeting therapeutics: molecular mechanisms of antisense oligonucleotides as a therapeutic platform. *Annu. Rev. Pharmacol. Toxicol.* **2010**, *50*, 259−293.

(15) Pifer, R.; Greenberg, D. E. Antisense antibacterial compounds. *Transl. Res.* **2020**, *223*, 89−106. Published Online: Jun. 6, 2020

(16) Alhamadani, F.; Zhang, K.; Parikh, R.; Wu, H.; Rasmussen, T. P.; Bahal, R.; Zhong, X.-B.; Manautou, J. E. Adverse Drug Reactions and Toxicity of the Food and Drug Administration-Approved Antisense Oligonucleotide Drugs. *Drug Metab. Dispos.* **2022**, *50* (6), 879−887, DOI: 10.1124/dmd.121.000418. Published Online: Feb. 27, 2022

(17) Kotil, S.; Jakobsson, E. Rationally designing antisense therapy to keep up with evolving bacterial resistance. *PLoS One* **2019**, *14* (1), No. e0209894. Published Online: Jan. 15, 2019

(18) Wu, S.; Gan, T.; Xie, L.; Deng, S.; Liu, Y.; Zhang, H.; Hu, X.; Lei, L. Antibacterial performance of graphene oxide/alginate-based antisense hydrogel for potential therapeutic application in *Staphylococcus aureus* infection. *Biomater. Adv.* **2022**, *141*, No. 213121. Published Online: Sep. 15, 2022

(19) Wurster, C. D.; Ludolph, A. C. Nusinersen for spinal muscular atrophy. *Ther. Adv. Neurol. Disord.* **2018**, *11*, No. 1756285618754459. Published Online: Mar. 13, 2018

(20) Zhou, K.; Li, C.; Chen, D.; Pan, Y.; Tao, Y.; Qu, W.; Liu, Z.; Wang, X.; Xie, S. A review on nanosystems as an effective approach against infections of *Staphylococcus aureus*. *Int. J. Nanomed.* **2018**, *13*, 7333−7347. Published Online: Nov. 9, 2018

(21) Ye, H.; Chu, X.; Cao, Z.; Hu, X.; Wang, Z.; Li, M.; Wan, L.; Li, Y.; Cao, Y.; Diao, Z.; Peng, F.; Liu, J.; Xu, L. A Novel Targeted Therapy System for Cervical Cancer: Co-Delivery System of Antisense LncRNA of MDC1 and Oxaliplatin Magnetic Thermo-sensitive Cationic Liposome Drug Carrier. *Int. J. Nanomed.* **2021**, *16*, 1051−1066. Published Online: Feb. 11, 2021

(22) Pritchard, N.; Kaitu'u-Lino, T.; Harris, L.; Tong, S.; Hannan, N. Nanoparticles in pregnancy: the next frontier in reproductive therapeutics. *Hum. Reprod. Update* **2021**, *27* (2), 280−304.

(23) Chen, Z.; Hu, Y.; Meng, J.; Li, M.; Hou, Z.; Zhou, Y.; Luo, X.; Xue, X. Efficient Transfection of Phosphorothioate Oligodeoxyribonucleotides by lipofectamine2000 into Different Bacteria. *Curr. Drug Delivery* **2016**, *13* (5), 784−793.

(24) Sriwidodo; Umar, A. K.; Wathoni, N.; Zothantluanga, J. H.; Das, S.; Luckanagul, J. A. Liposome-polymer complex for drug delivery system and vaccine stabilization. *Heliyon* **2022**, *8* (2), No. e08934. Published Online: Feb. 12, 2022

(25) Zhang, Y.; Ma, W.; Zhu, Y.; Shi, S.; Li, Q.; Mao, C.; Zhao, D.; Zhan, Y.; Shi, J.; Li, W.; Wang, L.; Fan, C.; Lin, Y. Inhibiting Methicillin-Resistant *Staphylococcus aureus* by Tetrahedral DNA Nanostructure-Enabled Antisense Peptide Nucleic Acid Delivery. *Nano Lett.* **2018**, *18* (9), 5652−5659. Published Online: Aug. 13, 2018

(26) Xue, X.; Mao, X.; Zhou, Y.; Chen, Z.; Hu, Y.; Hou, Z.; Li, M.-K.; Meng, J.-R.; Luo, X.-X. Advances in the delivery of antisense oligonucleotides for combating bacterial infectious diseases. *Nanomed. Nanotechnol., Biol. Med.* **2018**, *14* (3), 745−758. Published Online: Jan. 16, 2018

(27) Hu, Y.; Chen, Z.; Mao, X.; Li, M.; Hou, Z.; Meng, J.; Luo, X.; Xue, X. Loop-armed DNA tetrahedron nanoparticles for delivering antisense oligos into bacteria. *J. Nanobiotechnol.* **2020**, *18* (1), 109. Published Online: Aug. 4, 2020

(28) Yokoi, Y.; Kawabuchi, Y.; Zulmajdi, A. A.; Tanaka, R.; Shibata, T.; Muraoka, T.; Mori, T. Cell-Penetrating Peptide-Peptide Nucleic Acid Conjugates as a Tool for Protein Functional Elucidation in the Native Bacterium. *Molecules* **2022**, *27* (24), No. 8944, DOI: 10.3390/molecules27248944.

(29) Tréhin, R.; Merkle, H. P. Chances and pitfalls of cell penetrating peptides for cellular drug delivery. *Eur. J. Pharm. Biopharm.* **2004**, *58* (2), 209−223.

(30) Yazdi, M. E. T.; Qayoomian, M.; Beigoli, S.; Boskabady, M. H. Recent advances in nanoparticle applications in respiratory disorders: a review. *Front. Pharmacol.* **2023**, *14*, No. 1059343. Published Online: Jul. 19, 2023

(31) Chen, Z.; Hu, Y.; Mao, X.; Nie, D.; Zhao, H.; Hou, Z.; Li, M.; Meng, J.; Luo, X.; Xue, X. Amphipathic dendritic poly-peptides carrier to deliver antisense oligonucleotides against multi-drug resistant bacteria in vitro and in vivo. *J. Nanobiotechnol.* **2022**, *20* (1), 180. Published Online: Apr. 2, 2022

(32) Srijampa, S.; Buddhisa, S.; Ngernpimai, S.; Leelayuwat, C.; Proungvitaya, S.; Chompoosor, A.; Tippayawat, P. Influence of Gold Nanoparticles with Different Surface Charges on Localization and Monocyte Behavior. *Bioconjugate Chem.* **2020**, *31* (4), 1133−1143. Published Online: Mar. 25, 2020

(33) Faria, R.; Paul, M.; Biswas, S.; Vivès, E.; Boisguérin, P.; Sousa, Â.; Costa, D. Peptides vs. Polymers: Searching for the Most Efficient Delivery System for Mitochondrial Gene Therapy. *Pharmaceutics* **2022**, *14* (4), 757 DOI: 10.3390/pharmaceutics14040757.

(34) Hao, F.; Li, Y.; Zhu, J.; Sun, J.; Marshall, B.; Lee, R. J.; Teng, L.; Yang, Z.; Xie, J. Polyethylenimine-based Formulations for Delivery of Oligonucleotides. *Curr. Med. Chem.* **2019**, *26* (13), 2264−2284.

(35) Barrows, J. M.; Goley, E. D. FtsZ dynamics in bacterial division: What, how, and why? *Curr. Opin. Cell Biol.* **2021**, *68*, 163−172. Published Online: Nov. 18, 2020

(36) Han, H.; Wang, Z.; Li, T.; Teng, Da.; Mao, R.; Hao, Y.; Yang, N.; Wang, X.; Wang, J. Recent progress of bacterial FtsZ inhibitors with a focus on peptides. *FEBS J.* **2021**, *288* (4), 1091−1106. Published Online: Aug. 2, 2020

(37) CLSI. M100: Performance Standards for Antimicrobial Susceptibility Testing 28th ed.

(38) Alfei, S.; Schito, A. M. From Nanobiotechnology, Positively Charged Biomimetic Dendrimers as Novel Antibacterial Agents: A Review. *Nanomaterials* **2020**, *10* (10), No. 2022, DOI: 10.3390/nano10102022.

(39) Møller, P.; Lykkesfeldt, J. Positive charge, negative effect: the impact of cationic nanoparticles in the brain. *Nanomedicine* **2014**, *9* (10), 1441−1443.

(40) Crooke, S. T. Molecular Mechanisms of Antisense Oligonucleotides. *Nucleic Acid Ther.* **2017**, *27* (2), 70−77. Published Online: Jan. 12, 2017

(41) Bai, H.; You, Y.; Yan, H.; Meng, J.; Xue, X.; Hou, Z.; Zhou, Y.; Ma, X.; Sang, G.; Luo, X. Antisense inhibition of gene expression and growth in gram-negative bacteria by cell-penetrating peptide conjugates of peptide nucleic acids targeted to rpoD gene. *Biomaterials* **2012**, *33* (2), 659−667. Published Online: Oct. 14, 2011

(42) Meng, J.; He, G.; Wang, H.; Jia, M.; Ma, X.; Da, F.; Wang, N.; Hou, Z.; Xue, X.; Li, M.; Zhou, Y.; Luo, X. Reversion of antibiotic resistance by inhibiting mecA in clinical methicillin-resistant *Staphylococci* by antisense phosphorothioate oligonucleotide. *J. Antibiot.* **2015**, *68* (3), 158−164. Published Online: Oct. 1, 2014

(43) Hymel, H. C.; Rahnama, A.; Sanchez, O. M.; Liu, D.; Gauthier, T. J.; Melvin, A. T. How Cargo Identity Alters the Uptake of Cell-Penetrating Peptide (CPP)/Cargo Complexes: A Study on the Effect of Net Cargo Charge and Length. *Cells* **2022**, *11* (7), No. 1195, DOI: 10.3390/cells11071195.

(44) Lyu, T. S.; Ahn, Y.; Im, Y.-J.; Kim, S.-S.; Lee, K.-H.; Kim, J.; Choi, Y.; Lee, D.; Kang, E.; Jin, G.; Hwang, J.; Lee, S.-I.; Cho, J.-A. The characterization of exosomes from fibrosarcoma cell and the useful usage of Dynamic Light Scattering (DLS) for their evaluation.

PLoS One **2021**, *16* (1), No. e0231994. Published Online: Jan. 26, 2021

(45) Danaei, M.; Dehghankhold, M.; Ataei, S.; Davarani, F. H.; Javanmard, R.; Dokhani, A.; Khorasani, S.; Mozafari, M. R. Impact of Particle Size and Polydispersity Index on the Clinical Applications of Lipidic Nanocarrier Systems. *Pharmaceutics* **2018**, *10* (2), 57 DOI: 10.3390/pharmaceutics10020057.